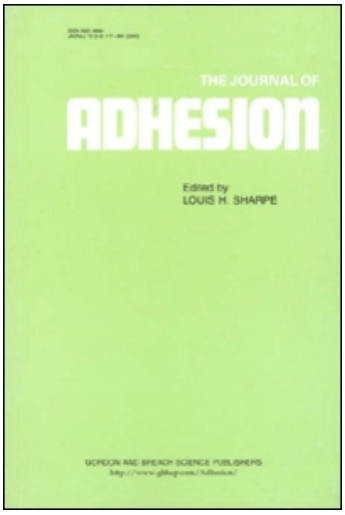

The Journal of Adhesion
Publication details, including instructions for authors and subscription information:
http://www.informaworld.com/smpp/title~content=t713453635

THERMALLY ACTIVATED PARAMETERS OF SELF-ADHESION IN ACRYLIC PRESSURE-SENSITIVE ADHESIVE-LIKE NETWORKS

Yev S. Garif[a]; William W. Gerberich[a]; Alphonsus V. Pocius[b]
[a] Department of Chemical Engineering and Materials Science, Minneapolis, Minnesota, USA [b] Corporate Research Laboratory, 3M Company, St. Paul, Minnesota, USA

Online publication date: 10 August 2010

To cite this Article Garif, Yev S. , Gerberich, William W. and Pocius, Alphonsus V.(2004) 'THERMALLY ACTIVATED PARAMETERS OF SELF-ADHESION IN ACRYLIC PRESSURE-SENSITIVE ADHESIVE-LIKE NETWORKS', The Journal of Adhesion, 80: 1, 61 — 85
To link to this Article: DOI: 10.1080/00218460490276786
URL: http://dx.doi.org/10.1080/00218460490276786

The Journal of Adhesion, 80: 61–85, 2004

ISSN: 0021-8464 print/1545-5823 online
DOI: 10.1080/00218460490276786

Taylor & Francis
Taylor & Francis Group

THERMALLY ACTIVATED PARAMETERS OF SELF-ADHESION IN ACRYLIC PRESSURE-SENSITIVE ADHESIVE-LIKE NETWORKS

Yev S. Garif
William W. Gerberich
Department of Chemical Engineering and Materials Science, University of Minnesota, Minneapolis, Minnesota, USA

Alphonsus V. Pocius
Corporate Research Laboratory, 3M Company, St. Paul, Minnesota, USA

We have conducted an experimental study of acrylic pressure-sensitive adhesive-like networks (PSA-LN) with the goal of establishing deconvolution of interfacial and bulk processes in adhesion. For contact adhesion testing, four types of cylindrically shaped samples were created, each synthetically modified to attain distinct bulk and surface properties. Introduction of small amounts of polar comonomers during synthesis increased the intrinsic adhesion energy, G_o, from 65 mJ/m^2 for an unmodified acrylic PSA-LN to 129, 158, and 218 mJ/m^2 for PSA-LNs modified with 10 wt% of acrylic acid, amino acrylate, and acrylonitrile comonomers, respectively. Following a reversed trend, the critical rate of separation, v^* (below which deadhesion is an intrinsically interfacial process) was more than halved from 496 nm/s for the unmodified PSA-LN to 201, 188, and 212 nm/s for those modified with the same three comonomers (same order, respectively).

Received 11 August 2003; in final form 12 November 2003.

One of a collection of papers honoring Jacob Israelachvili, the recipient in February 2003 of *The Adhesion Society Award for Excellence in Adhesion Science, Sponsored by 3M*.

The authors would like to thank Dr. Afshin Falsafi (3M) for constructing the JKR apparatus, Dr. Lihua Li (Advanced Materials) for producing results that motivated this work, Prof. Christopher W. Macosko (University of Minnesota) for critical feedback at the inception of the work, Dr. Phillip J. Cole (Sandia National Labs) for ongoing feedback and review of our previous publications, Dr. David Giles (University of Minnesota) for assistance with rheological measurements, and Mr. Gary Korba (3M) for XPS surface composition analysis. Support from the 3M Company for Y. S. Garif is appreciated, as is support from the NSF under Grant DMI-0103169 for W. W. Gerberich.

Address correspondence to Alphonsus V. Pocius, 3M Corporate Research Laboratory, 3M Center, Bldg. 201-4N-01, St. Paul, MN 55144–1000, USA. E-mail: avpocius1@mmm.com

The adhesion energy was found to be dependent upon the crack propagation rate and sensitive to it at all rates of interfacial separation, including those below the critical crack propagation rate, v^*. In addition, the dependence of the adhesion energy on crack propagation rate was measured at three temperatures. It was found that v^* displayed an Arrhenius dependence on temperature from which an activation energy could be calculated. Those activation energies, as a function of chemical composition, are compared with activation energies derived from shift factors determined from measurements of bulk modulus as a function of temperature. A direct correlation between those activation energies was noted.

Keywords: Polymer; Adhesion; Rate; Temperature; Interface; Length scale; Intermolecular interactions; Viscoelasticity; Adhesives

INTRODUCTION

The strength of an adhesive bond is most often found to be orders of magnitude in excess of the strengths of molecular attraction that occur at interfaces. Making the connection between those fundamental forces and adhesive bond strength is a goal that has been investigated by adhesion scientists since the 1950s. One of the first attempts to make this connection was proposed by Gent and Schultz [1]. This connection was also investigated by Kinloch and Andrews [2], resulting in a relationship of the following sort:

$$G = W_A(1 + \Phi(v, T)), \tag{1}$$

where G is the "adhesion energy" or work to break an adhesive bond, W_A is the reversible thermodynamic work of adhesion, Φ is a "loss function" that describes the dissipation of mechanical energy within the adhesive joint, v is a rate (of application of mechanical energy or of interfacial crack propagation), and T is the temperature. The primary difficulty in attempting to deconvolute these parameters from each other is that most tests of practical adhesive bond strength occur at rates that are far too fast and are thus dominated by Φ. Contact mechanical measurements of the sort described in this article allow us to interrogate the process of adhesive bond breakage at rates at which Φ becomes small.

The contact behavior of materials is a phenomenon with a long history of theory and research. A theory describing the contact of adhesionless elastic bodies of revolution pioneered by Hertz [3], triggered development of a new field known as "contact mechanics." During the twentieth century, a number of fundamental models added to the understanding of various types of contacts. Notably, the Bradley model [4] was the first to introduce a surface energy correction into

a simple elastic contact. The idea was further developed in the JKR model [5] and countered by the alternative DMT model [6] with a Dugdale-Barenblatt crack tip cohesive zone approach. To reconcile the two, Maugis introduced a broad theory [7] with a dimensionless parameter to reflect the length scale of deformation due to the range of adhesive forces. The model was further generalized to eliminate the assumption of elastic-only deformations. Thus, nonempirical modeling of plastic indentation [8] was proposed and solved numerically.

More recently, Shull and coworkers [9], as well as Li *et al.* [10], have examined the contact mechanics of acrylic networks. In general, it was found that the results could be modeled using the following relationship:

$$G = G_0\left(1 + \left(\frac{v}{v^*}\right)^n\right), \tag{2}$$

where G_0 is an "intrinsic adhesion energy," v^* is a "critical crack propagation rate," and n is a power law index. v^* and n can also be considered to be fitting parameters. For some data, the critical crack propagation rate can be seen as an abrupt change in slope when log G is plotted *versus* log v. It is apparent that Φ in Equation (1) has been replaced by terms containing the rates of interfacial crack propagation (v and v^*). Φ is expected to be temperature dependent, but Equation (2) contains no explicit relationship to temperature. Accordingly, it is a goal of this experimental study to explore the temperature dependence of the terms in Equation (2), thus providing more insight into the relationship of interfacial forces and adhesive bond strength. A technique employing normal contact of cylindrically shaped, essentially elastic, acrylic samples has been utilized to interrogate adhesion behavior at different temperatures. Corresponding bulk mechanical properties and surface composition were independently characterized to support the analysis of the adhesion results. Findings of this study provide insight into the energetics of processes controlling adhesive response.

EXPERIMENTAL

Model Systems

Acrylic pressure-sensitive adhesives (PSAs) were chosen as model polymer systems. PSAs are well-known articles of commerce, thus providing relevance for the work. They were chosen for the relative ease of synthetically attaining surface and rheological properties desired for adhesion testing within the accessible temperature range of our

laboratory equipment. The inherent viscoelastic nature of acrylic PSAs was significantly suppressed by the addition of a crosslinker into the monomer mixture. Accordingly, the resulting elastomers are referred to as PSA-like networks or PSA-LNs, in line with terminology introduced earlier in a similar study [10a].

The PSA-LNs in this study were synthesized from 80–90 wt% 2-ethyl hexyl acrylate, 10 wt% hexanediol diacrylate, and 0–10 wt% polar comonomer. Comonomers were added to modify the surface energy and rheological properties of the resulting samples [11]. Table 1 lists specific chemicals and their roles in the synthesis of the acrylic PSA-LNs.

Sample preparation was performed in three steps. First, every chemical was purified to remove polymerization inhibitors. Filtering the monomers through molecular-sieve packed columns and then purging them with high purity argon to eliminate remaining oxygen, which can also act as an inhibitor, accomplished this. Second, the purified chemicals were placed in an argon-purged glove box where they

TABLE 1 List of Chemicals Used to Synthesize Acrylic PSA-LNs

Main bulk monomer for all samples:

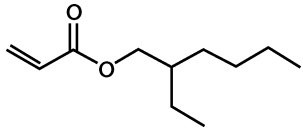

2-ethyl hexyl acrylate (**EHA**)
Polar comonomers (modifiers):

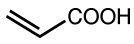

acrylic acid (**AA**)

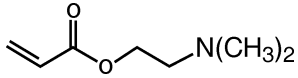

di-methyl amino ethyl acrylate (**DMAEA**)

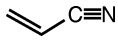

acrylonitrile (**AN**)
Crosslinker

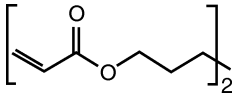

1,6-hexanediol diacrylate (**HDDA**)

TABLE 2 Composition of synthesized acrylic PSA-LNs. Note the sample designations that are used throughout this paper. Abbreviations for monomer names are explained in Figure 1

Sample designation	Monomer (wt%)	Comonomers (wt%)			Crosslinker (wt%)
	2-EHA	AA	DMAEA	AN	HDDA
PSA-LN-NoAA	90	—	—	—	10
PSA-LN-10AA	80	10	—	—	10
PSA-LN-10DMAEA	80	—	10	—	10
PSA-LN-10AN	80	—	—	10	10

were mixed at the compositions shown in Table 2. After addition of 0.2 wt% of a free-radical initiator, azo-bis-isobutyronitrile (AIBN), the mixtures were transferred into capillary tubes that were sealed with rubber caps. Finally, the capped tubes were taken out of the glove box into a convection oven to polymerize the mixtures at about 80°C for at least 24 h. PSA-LN cylinders were formed inside each capillary tube. As a result of polymerization shrinkage, the cylinders were easily released by shattering the fragile tubes. Soaking and washing the cylindrical samples in ethyl acetate, a solvent that swells acrylic networks, removed the bits of glass stuck on the PSA-LN surface. During the subsequent 48 h, the cylinders were slowly dried in closed glass Petri dishes to assure gradual evaporation of the solvent. Rapid drying could result in surface cracking due to uneven shrinkage of the elastomer network as the solvent escaped.

When the samples were finally dry and ready for handling, they were analyzed with X-ray photoelectron spectroscopy (XPS) to confirm that their surface composition was indeed in agreement with expectations from the synthesis procedure. Table 3 summarizes XPS results for the four types of PSA-LN cylinders prepared for adhesion testing. In general, it was found that the surface composition agreed well with that expected for these materials, with a slight excess of carbon. For materials that contain a significant amount of alkyl side-chains, a slight segregation of hydrocarbons to the surface is to be expected.

Dynamic Mechanical Testing

The last step before adhesion testing was measurement of dynamic *bulk* mechanical properties of the cylindrical samples. Information acquired during this step was essential for both validation of the adhesion test results and relating interfacial and bulk phenomena in

TABLE 3 Surface Elemental Composition of PSA-LNs

	XPS measured (%)			Synthesis predicted (%)		
Sample designation	C	O	N	C	O	N
PSA-LN-NoAA	83.8	15.5	—	84.8	15.2	—
PSA-LN-10AA	80.4	19.8	—	79.3	20.6	—
PSA-LN-10DMAEA	83.4	15.6	1.4	83	15.8	1.2
PSA-LN-10AN	78.6	14.7	3.4	76.6	11	5.1

The measured values are compared to calculated values assuming the surface and bulk composition to be the same. XPS error is $\pm 2\%$.

adhesion. During adhesion measurement, the contact produces predominantly compressive stresses. Accordingly, dynamic mechanical measurements were done in compression. The synthesized PSA-LN cylinders were placed vertically between the plates of a rheometer. To identify the glass transition temperature and relaxation times at various temperatures, both frequency and temperature sweeps were performed. Dynamic mechanical spectra taken at 1 Hz as a function of temperature for the four types of PSA-LNs are shown in Figures 1a to 1d. The glass transition temperatures are all below room temperature. We also note that the modulus above room temperature rises as a function of temperature, as would be expected for an elastic network [12]. Time–temperature superposition was done to obtain shift factors as a function of temperature, which, if analyzed in Arrhenius form, gives a measure of the activation energy for polymer motion. A representative set of shift factor data is shown in Figure 2.

Normal Contact Adhesion Testing

After bulk and surface properties were measured, cylindrical PSA-LN samples of the same diameter were crossed at 90° and brought in and out of contact to measure adhesion processes. The overall apparatus was described by Falsafi *et al.* [13]. A schematic of a portion of our instrument is shown in Figure 3. One PSA-LN cylinder was glued with epoxy to a glass slide firmly attached to the metal fixture of a high-precision micrometer. Another cylinder was glued to a silicon wafer attached to a scale having four decimal place accuracy. Accordingly, the micrometer controls the displacement of the upper sample (input) while the scale measures the contact load (output). Not shown is a microscope with a video camera that is mounted vertically above the glass slide to monitor the size of the contact circle (also recorded

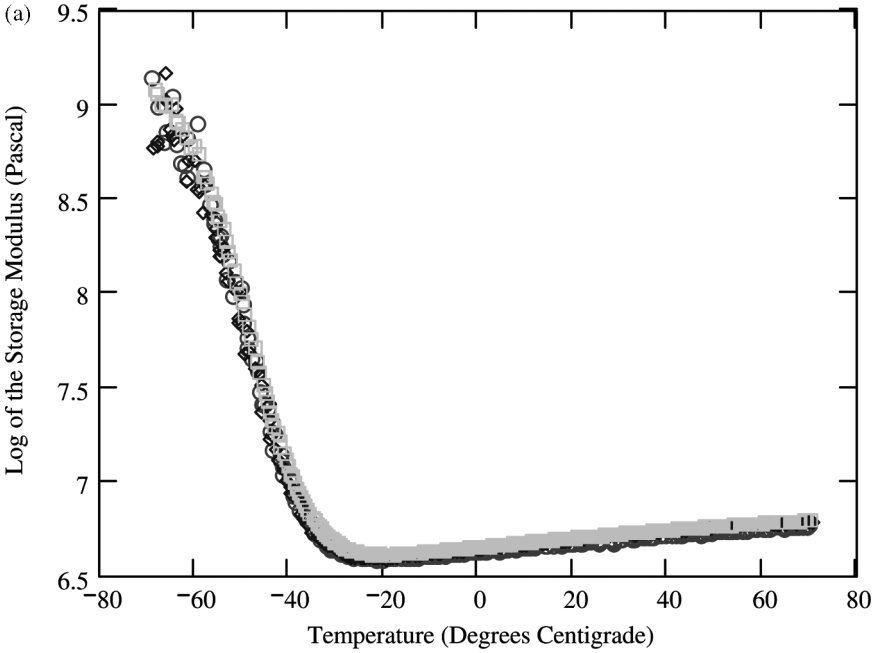

FIGURE 1 Dynamic mechanical spectra for PSA-LNs taken as a function of temperature. The frequency of test was 1 Hertz: (a) PSA-LN-NoAA, (b) PSA-LN-10DMAEA, (c) PSA-LN-10AN, and (d) PSA-LN-10AA. (Continued.)

output) as it expands during loading and shrinks during separation (unloading.) The samples were held in a thermostatically controlled chamber through which cooled or warmed dry nitrogen was passed.

Johnson, Kendall, and Roberts (JKR) provided a contact mechanical theory best suited for analytical interpretation of force-contact area profiles of soft (low elastic modulus) materials with the size of the contact much greater than that of the cohesive zone along the rim of the contact [5]. This theory was used to analyze our raw adhesion data for acrylic PSA-LNs under loading conditions. Of main interest to this study is the process of unloading. A sample loading–unloading profile is shown in Figure 4.

The loading portion of the data is fit to the JKR theory in Equation (3),

$$a^3 = \frac{R}{K}\left(P + 3\pi W_A R + \sqrt{6W_A RP + (3\pi W_A R)^2}\right), \tag{3}$$

by finding proper values for the parameters K, the elastic constant,

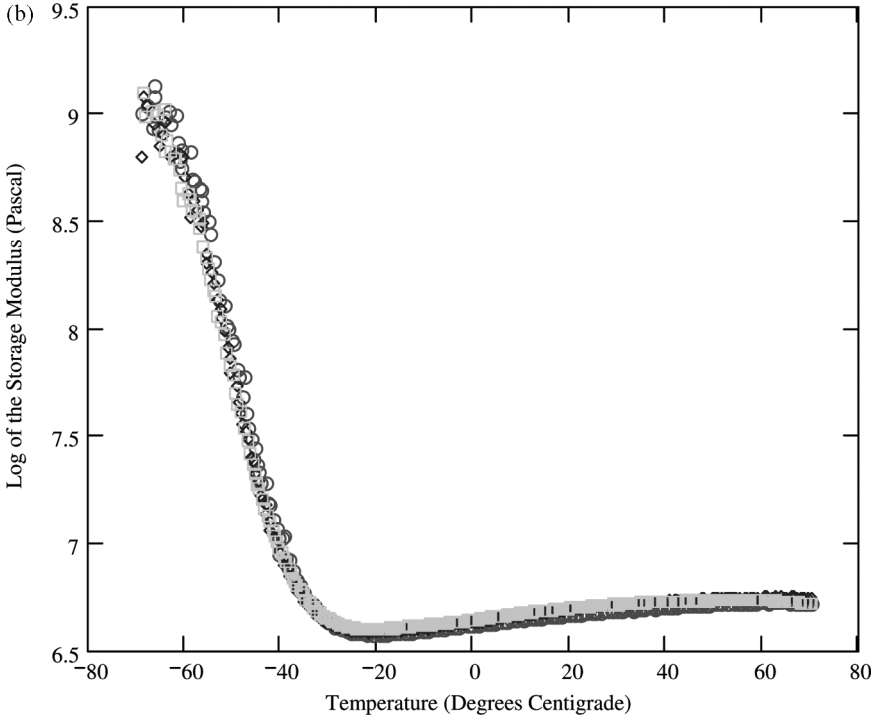

FIGURE 1 (Continued.)

and W_A, the work of adhesion. P is the applied load. R and K are defined by

$$\frac{1}{R} = \frac{1}{R_1} + \frac{1}{R_2},$$
$$\frac{1}{K} = \frac{3}{4}\left(\frac{1-\varepsilon_1^2}{E_1} + \frac{1-\varepsilon_2^2}{E_2}\right),$$

where the R_i are the radii of the two contacting cylinders, and the E_i and the ε_i are the moduli and Poisson's ratio of the two contacting cylinders, respectively. Values of R were obtained by measurement. K and W_A are essentially fitting parameters for a^3 *versus* P data. Magnitudes of the elastic constants obtained through fitting the data using the JKR theory were in close agreement with those derived from storage moduli measured rheometrically. Thus, both sets of data were mutually validated. It should be noted, however, that magnitudes of the work of adhesion (by definition, twice the surface energy, γ_S) were

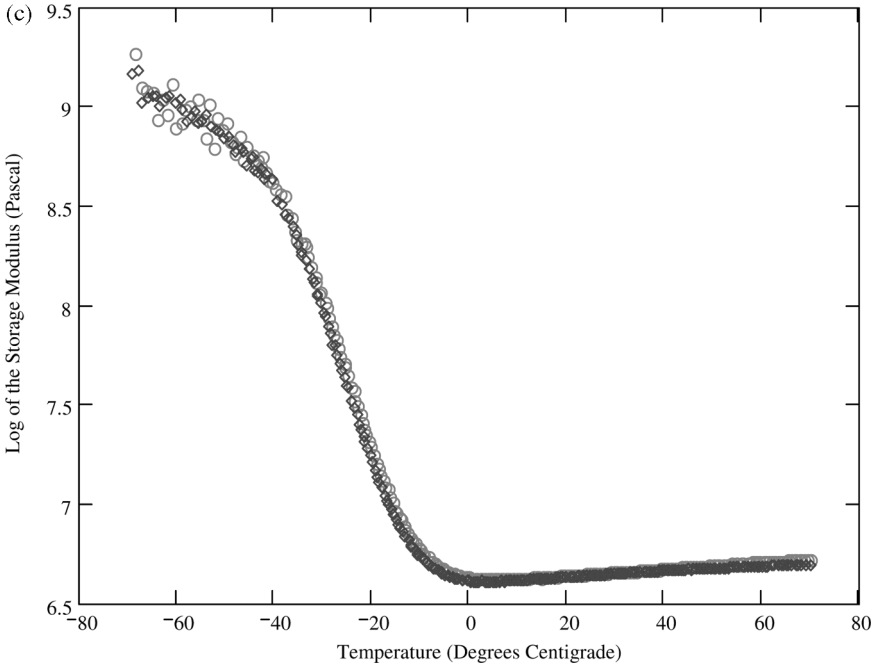

FIGURE 1 (Continued.)

not independently verified, assuming that rheological validation of the data was sufficient to prove the validity of the use of the JKR equation.

Maugis [7] rearranged the JKR equation as shown in Equation (4), which gives the adhesion energy, G, as a function of load and radius:

$$G = \frac{\left(\frac{a^3K}{R} - P\right)^2}{6\pi a^3 K}. \tag{4}$$

Equation (4) was used to analyze the unloading data. Values of G were calculated for each unloading data point. The crack propagation rate was determined by measuring the radius at two consecutive times, taking their difference and dividing by the time elapsed between measurements. The G value for such data was taken as the average of the G values for consecutive measurements of a.

In order to understand better the contact between two cylinders, one can view the contact as a circular crack pointing inward with its tip located at the circumference of the contact. As the cylinders are pressed against each other, the contact becomes larger, making the crack heal outward. Consequently, during unloading of the cylinders

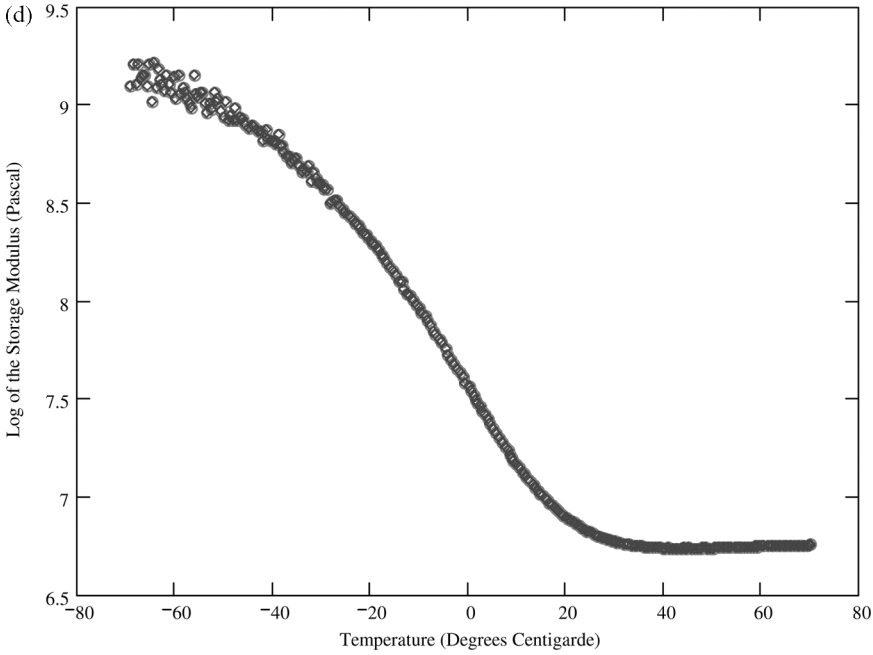

FIGURE 1 (Continued.)

the contact shrinks back to smaller dimensions, driving the crack to propagate inward. Due to the finite curvature of cylindrical surfaces, a steady rate of unloading in a direction normal to the contact does not translate into a steady rate of the movement of the contact front (crack tip). Thus, a crack associated with a small contact (barely touching) propagates faster because the crack mouth around the contact is more converging than in the case of cylinders with more contact. On the other hand, cylinders of smaller radius of curvature with the same size of the contact would drive the crack faster for the same normal displacement because smaller cylinders make the crack mouth more open, or less converging.

Close inspection of the data in Figure 5 shows that the crack propagation rate, v, at which the contact radius changes can be accurately traced throughout the test for all contact sizes. Because all data points during JKR tests are recorded at a steady acquisition frequency, their density along the contact radius axis reflects the crack propagation rate. In other words, one test produces a data series with a wide range of rates. The larger the distance between two points in terms of the contact radius, the faster is the average rate at which the crack tip

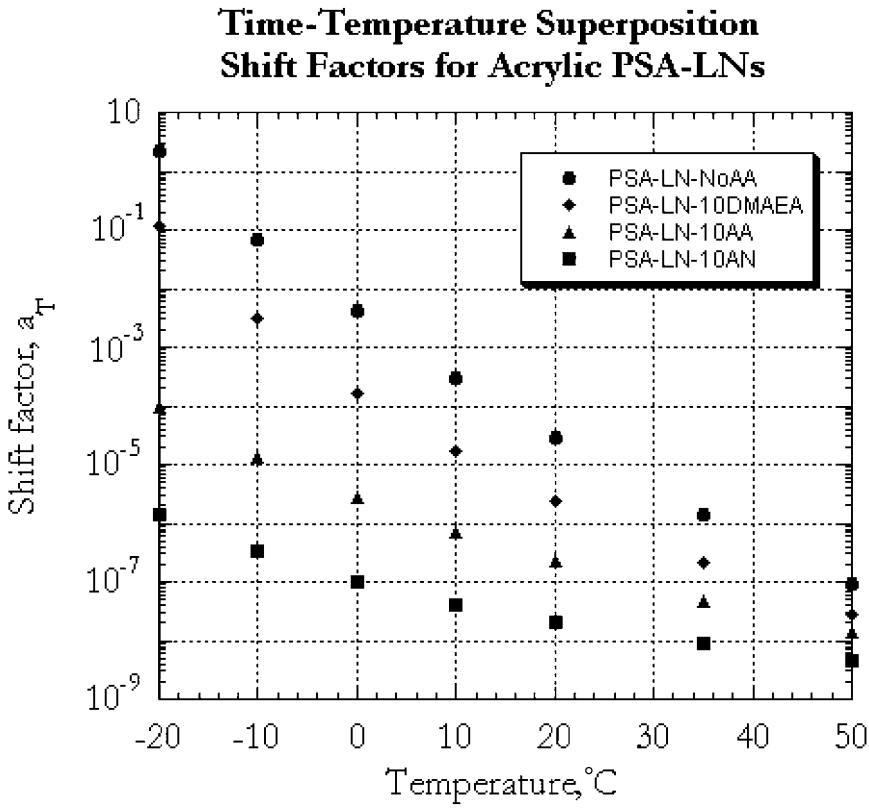

FIGURE 2 The sets of shift factors shown have arbitrary values only to show relative change with temperature and that the systems tested are well behaved.

moves between these points. As seen in Figure 5, slow crack propagation rate data are more abundant and, therefore, more statistically reliable than the fast ones. When the entire data set is plotted along a logarithmic axis, the difference in data density is not as apparent due to logarithmically stronger compression of the data at higher rates. In fact, the overall distribution of crack propagation rates plotted logarithmically appears relatively uniform, as shown in Figure 6.

RESULTS

Table 4 summarizes the bulk and interfacial properties for each of the four systems tested at room temperature. It highlights trends in these

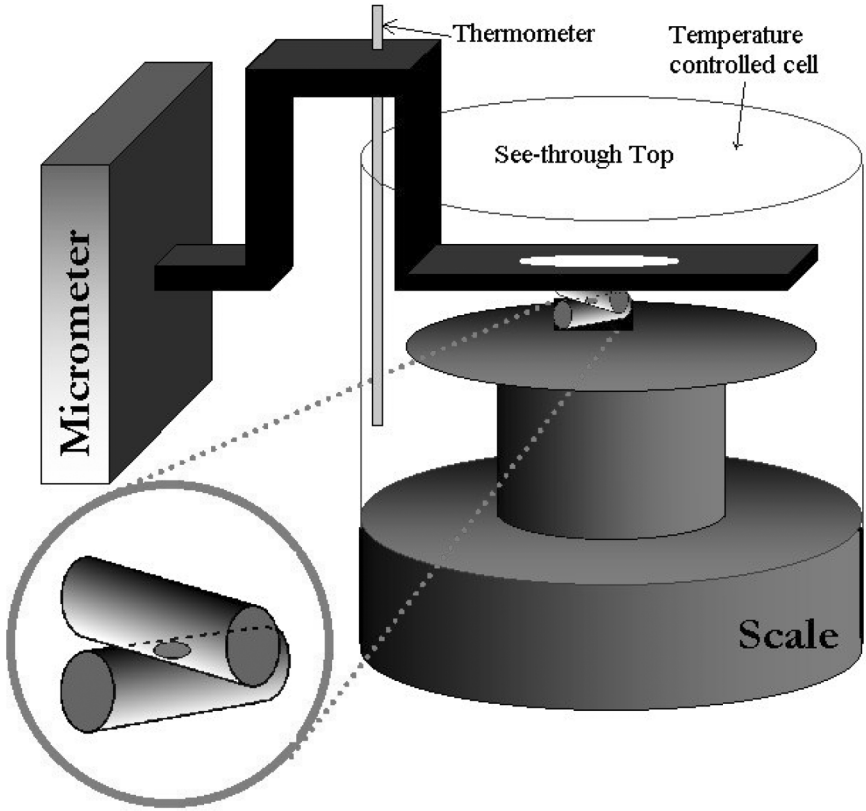

FIGURE 3 Schematic of the custom-made, temperature-controlled apparatus used for the contact testing of adhesion between acrylic PSA-LN cylinders.

properties due to the difference in composition. We note that the bulk room temperature modulus of these materials does not vary significantly despite the differences in their chemical composition. Table 4 provides values of the Work of Adhesion, W_A, as determined from fitting the data obtained from the loading portion of the experiment and the JKR Equation (Equation (3)). We can calculate the surface energy of the materials used by dividing the W_A by 2.

Adhesion behavior was measured at three test temperatures. The entire set of the contact mechanics data measured in this work is shown in Figure 6. For each acrylic PSA-LN, a transition of G as a function of v was identified at each temperature. This transition is given the name v^*. A sample data set identifying the transition for each of the four systems tested at room temperature is shown in

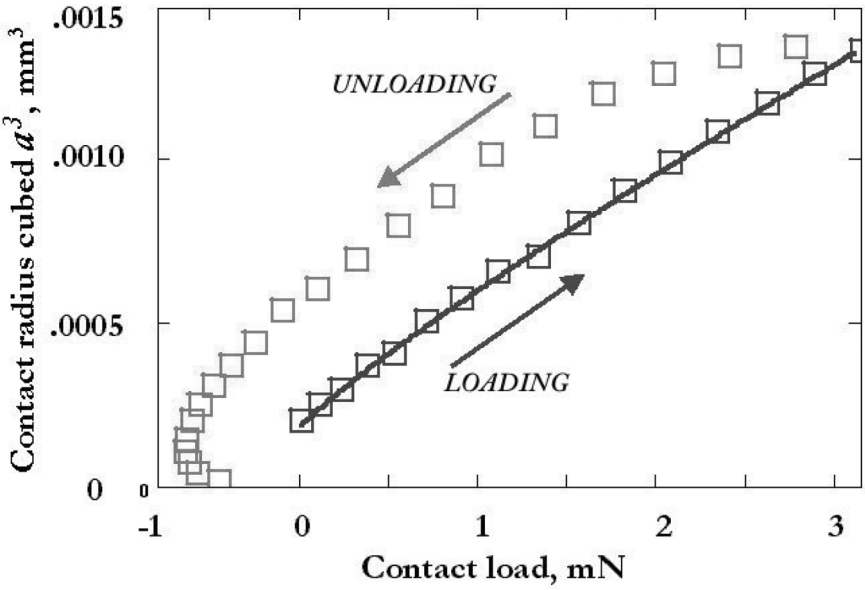

FIGURE 4 A typical JKR plot for data taken in this work. The loading data are used to obtain a value of W_A and K. The fact that the unloading data do not superimpose on the loading data indicates that the process is hysteretic, *i.e.*, it takes more energy to separate the samples than it does to bring them into contact. The unloading data are used to determine adhesion energy as a function of crack propagation rate.

Figure 7. The transition is obvious for PSA-LN-NoAA and PSA-LN-10AN but less so for the other two systems. We performed a linear regression of log G *versus* v below v^* and extrapolated to zero rate to provide the value of G_0. The statistical "R value" (not to be confused with R in the JKR equation) for these linear regressions was 0.88, or higher for all but two of the analyses. These two had R values of about 0.75. The value of G_0 is, in all cases, higher than W_A.

In contrast, the high rate end of the data clearly shows how much faster G is changing with v beyond v^*. At the high rates, a linear regression of *log G versus log v* was done. The intersection of these two linear regressions of the data provided our value of v^*. Values of v^* at room temperature are shown in Table 4. For each of the four PSA-LN systems, the data above v^* have a power law index less than unity (the values are shown in Figure 8). The values of n range from 0.4–0.8 depending upon temperature, with room temperature values of about 0.6, consistent with previous results [10(a)]. To be sure, there

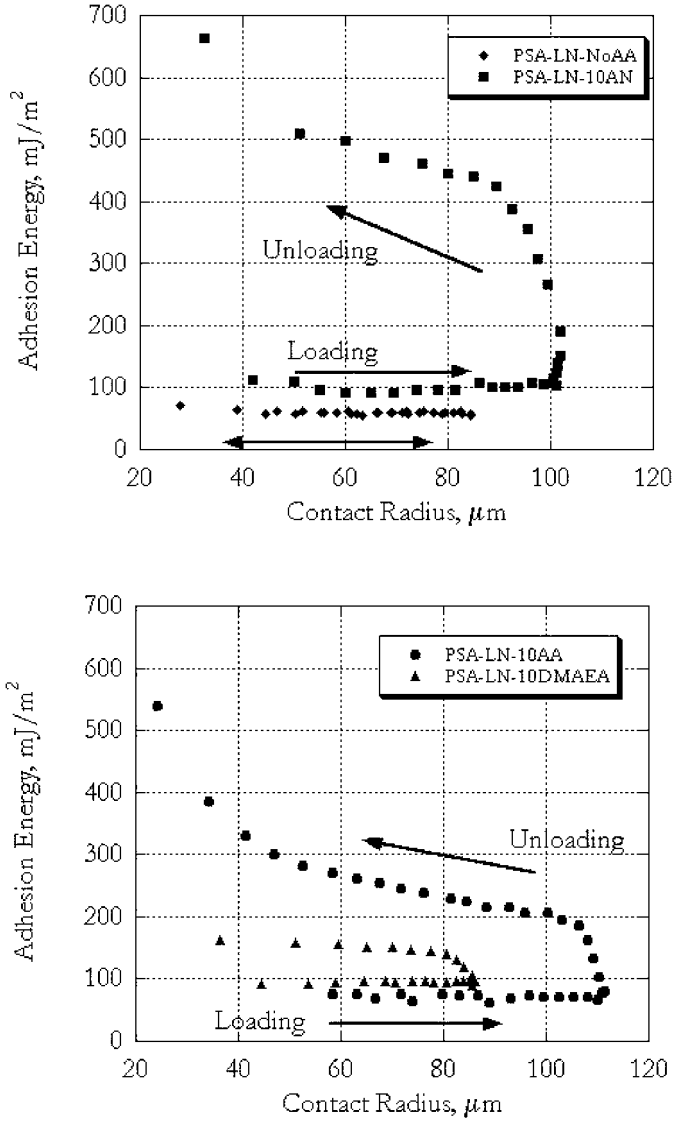

FIGURE 5 Sample data set showing the difference between the loading adhesion energy (lower plateau) and the adhesion energy from unloading (upper portion of the data) for the four PSA-LNs used in this work. Note that PSA-LN-NoAA shows essentially no hysteresis but the other systems show measurable hysteresis.

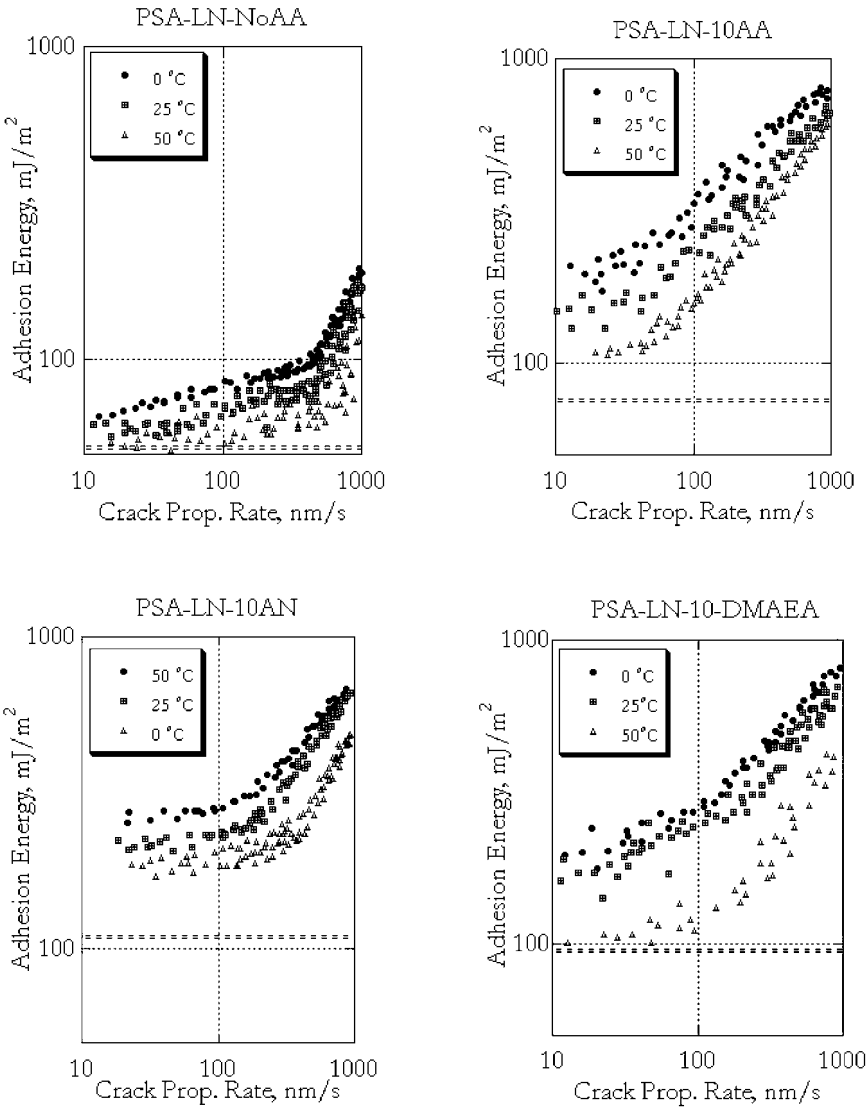

FIGURE 6 The entire data set for all of the systems tested at all temperatures showing the variation of G with crack propagation rate. Note that as temperature is increased, the curves appear to shift to the right (faster rates) and down (lower energy). The dashed lines indicate the approximate location of the thermodynamic work of adhesion, measured at room temperature.

TABLE 4 Room Temperature Properties of Acrylic PSA-LNs

	Interfacial properties			Bulk properties	
Sample designation	W, mJ/m^2	G_o, mJ/m^2	v^*, nm/s	E', MPa	T_g,°C
PSA-LN-NoAA	59 ± 5	65 ± 5	496 ± 43	4.73 ± .08	−45 ± 2
PSA-LN-10AA	73 ± 5	129 ± 7	201 ± 32	4.25 ± .06	−10 ± 2
PSA-LN-10DMAEA	93 ± 5	158 ± 12	188 ± 28	5.03 ± .04	−40 ± 6
PSA-LN-10AN	107 ± 5	218 ± 15	212 ± 35	4.48 ± .06	−20 ± 2

The work of adhesion, W_A, from JKR fit on loading; intrinsic adhesion energy, G_o, extrapolated from JKR adhesion data during unloading; characteristic crack propagation rate, v^*, from transition from low to high power law of adhesion; bulk storage modulus, E'; glass transition temperature, T_g.

are insufficient data to be confident of the value of n because less than a decade of rate is available for most of the systems examined. In fact, the initial reason for examining temperature dependence was to attempt a time–temperature superposition of data to provide an extension of the range of rates. Because of the vertical shifts noted in this work (see Figure 6), this was not possible.

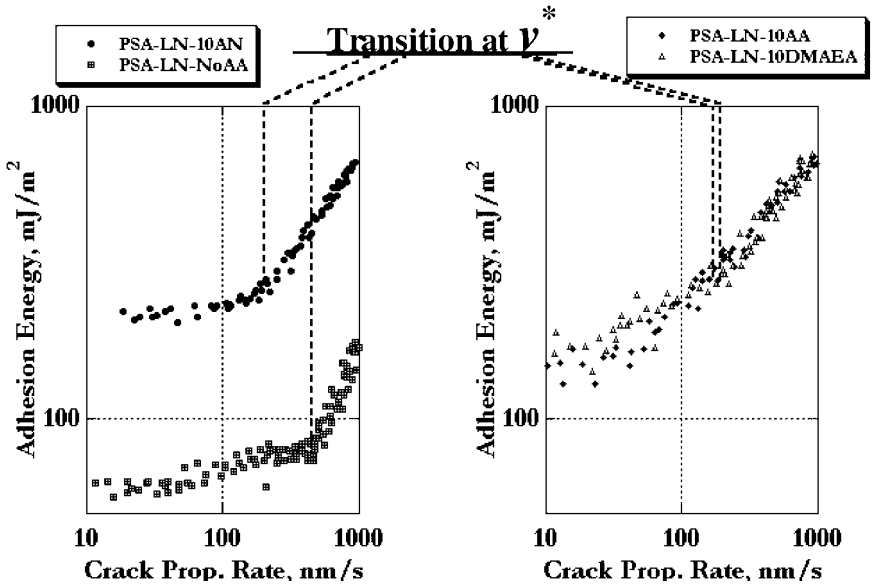

FIGURE 7 Plots of log G *versus* log v for the four systems used in this work measured at room temperature showing the position of v^*.

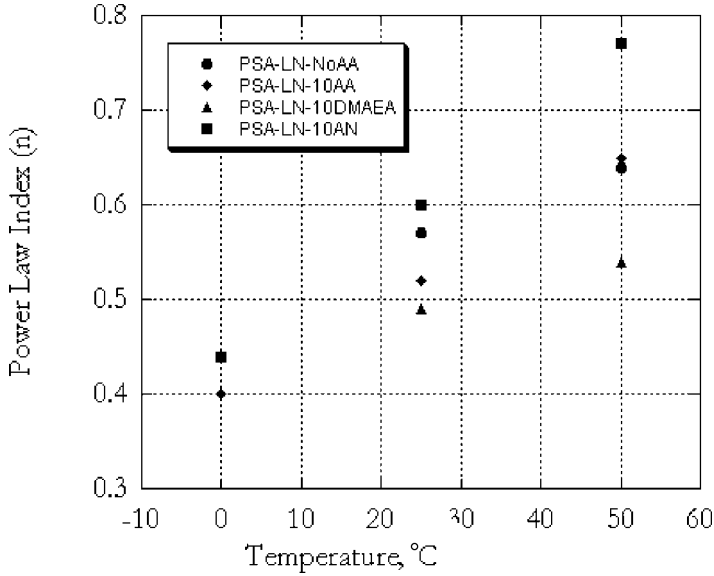

FIGURE 8 A plot showing the variation of the power law index (n) as a function of temperature. This power law index was determined by a linear regression of log *G versus v* above v^*.

We also analyzed our data using Equation (2). A generalized least-squares fit of the data to Equation (2) gave results that were physically unreasonable. A weighted generalized least-squares fit, in which the data at lower rates were given more weight, still did not provide physically reasonable fitting parameters. In general, our attempts to fit the data to Equation (2) resulted in higher values of G_0 than were obtained by our linear regression of the log *G versus v* data. The values of v^* obtained from the generalized least-squares fits of the data followed no obvious pattern, while the data show a pattern in which v^* increases with temperature. Thus, even though Equation (2) describes our data in the most general of senses, it does not predict all of the features that our data display. In general, this discrepancy is most obvious at the lower crack propagation rates. It is difficult to force Equation (2) into having a slope below v^* while at the same time having a power law behavior above v^*. Thus, we use our linear regression scheme to arrive at values of G_0 and v^*.

Each system was tested at three temperatures. Twelve sets of measurements of v^* were generated, allowing us to examine the nature of this fundamental adhesion parameter. The most important finding of

this study is a measurable change in the critical rate, v^*, with temperature. The values of v^* can be plotted on a semilog plot *versus* reciprocal temperature (see Figure 9). According to the Arrhenius relationship, the slope of such a plot provides an activation energy ($Q_A(v^*)$) for the crack propagation process. The magnitude of the activation energies found may provide insight into the nature of the physical process(es) determining the adhesion response as a function of the chemistry of the sample. Each data point in Figure 9 is a result of multiple adhesion tests run at the three temperatures over a wide range of rates of separation. The statistical R value for the linear regression of the data in Figure 9 is given in Table 5. It shows the significance of the correlation. Bulk and adhesion responses were contrasted by comparing activation energies, $Q_A(v^*)$, with those of polymer motion derived from shift factors, $E_A(a_T)$. The latter were determined from temperature dependence of the time–temperature superposition shift factors (see the above section "Dynamic Mechanical Testing" and Figure 2). The $Q_A(v^*)$ and $E_A(a_T)$ are compared in Table 5.

DISCUSSION

This article is primarily concerned with the determination of the work of adhesion, W_A, intrinsic adhesion energy, G_0, and the dependence of adhesion energy, G, on crack propagation rate, v, and temperature. Our initial hope was to use the temperature dependence of G on v to generate a "master curve" of the adhesion properties of these systems. In that way, we hoped to extend the data in our previous publication [10] to effectively higher rates. We were not able to achieve this goal, but rather discovered some potentially more interesting fundamental findings.

Examination of the data presented in the previous section shows that the thermodynamic work of adhesion, as measured by the loading portion of this contact mechanical method, provides surface energy values that are similar to those that would be expected for materials of these chemistries. That is, they are on the order of 30–60 mJ/m^2 ($\gamma_S = W_A/2$). In contrast, the unloading data provide intrinsic adhesion energy, G_0,which is always higher than W_A. We believe that this "discrepancy" is not a measurement artifact, but rather that it represents a fundamental phenomenon that occurs at the interface between two materials when they are placed in contact. The work of adhesion describes the energetics of placing two materials into intimate contact when they were previously in contact with dry air. When in contact, the materials can rearrange (since, in this experiment, they are above their T_g) to come into a minimum energy state, providing a new

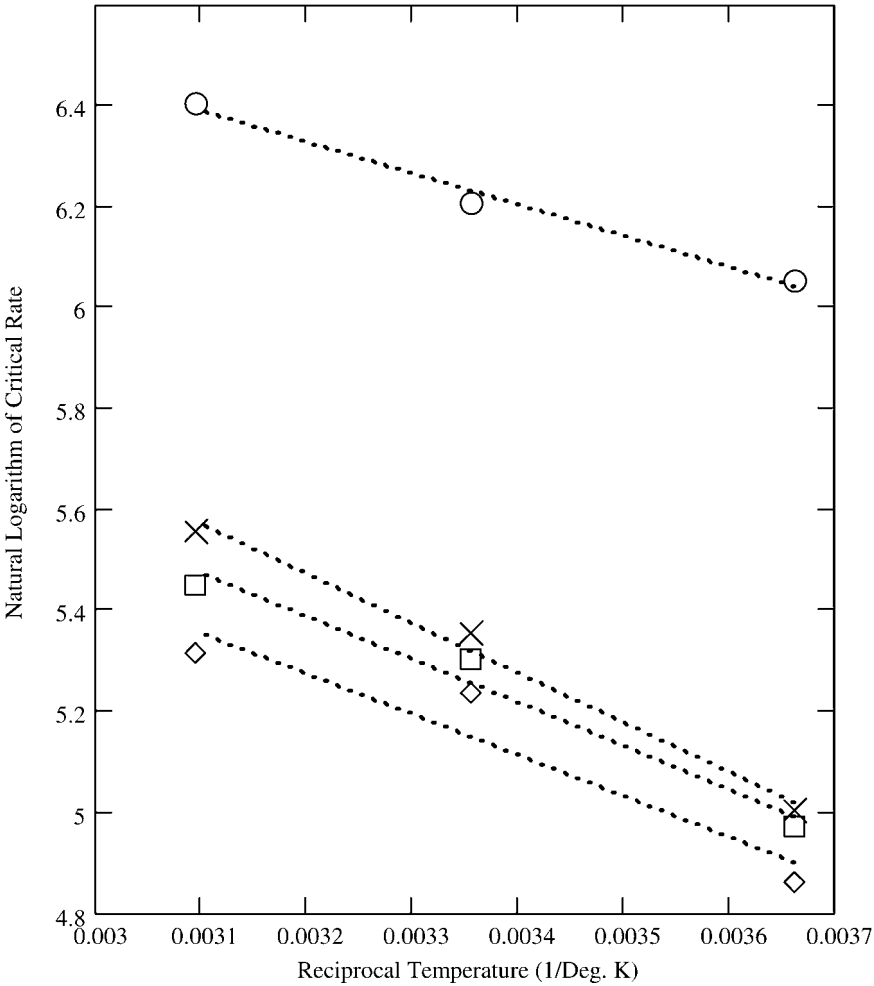

FIGURE 9 Plot showing the logarithm of the critical crack propagation rate as a function of reciprocal temperature, demonstrating the Arrhenius behavior of this parameter. Legend: Circles, PSA-LN-NoAA; X, PSA-LN-10AN; Squares, PSA-LN-10AA; Diamonds, PSA-LN-10DMAEA.

interface that is not a duplicate of the surfaces of the materials before they were brought into contact. Thus, the energy necessary to separate those materials, G_0, should not be W_A, but rather some other number that is significant to the materials after they have come into equilibrium after the interface was formed. The new data presented in this article further substantiate the findings in our previous

TABLE 5 Correlation Between Activation Energies for Bulk Polymer Motion, E_A, (Determined from Shifting Dynamic Mechanical Data) and Activation Energies for Interfacial Crack Propagation, $Q_A(v^*)$

Sample designation	$E_A(a_T)$ *kJ/mole*	$Q_A(v^*)$ *kJ/mole*	$Q_A(v^*)$ *kcal/mol*	Variance in the linear regression
PSA-LN-NoAA	106 ± 8	5.1 ± .7	1.2 ± 0.2	0.99303
PSA-LN-10DMAEA	100 ± 6	6.7 ± .8	1.6 ± 0.2	0.95037
PSA-LN-10AA	150 ± 13	7.2 ± .6	1.7 ± 0.1	0.98544
PSA-LN-10AN	168 ± 8	8.1 ± .9	2 ± 0.2	0.99427

The last column provides the variance for the linear regression used to determine Q_A.

publication [10(a)]. This phenomenon is known as "adhesion hysteresis", and a similar explanation was presented by Maeda *et al.* [14] and Ghatak *et al.* [16].

Figure 6 displays the data obtained for all four systems. Each curve shifts to the right (higher rates) and down (lower adhesion energy) as function of increasing temperature. The shape of the curves for each of the PSA-LNs appears as though a vertical as well as a horizontal shift factor could superimpose the data. That is, if one would shift each curve upward to match G_0 at 0°C and leftward to match v^*, the curves would approximately superimpose. As shown in Figure 9, the v^* data fit an Arrhenius relationship. Thus, the processes interrogated in these experiments appear to be thermally activated.

The experimental results reported in the previous section show that for all four types of acrylic PSA-LN cylinders tested, the thermodynamic work of adhesion obtained during elastic loading is lower than the intrinsic adhesion energy, G_0. A listing of all of the intrinsic adhesion energies determined in our work is given in Table 6. The variation in G_0 with temperature is also interesting. Wu has indicated that the surface energy of polymers should vary on the order of 0.1 mJ/m^2 deg [15]. The interfacial energy should vary less than that. The G_0 measured in our experiments varies by as much as 1.9 mJ/m^2 deg. The least variation occurs with the material containing no polar monomer, PSA-LN-NoAA. These findings indicate that even at near-zero rates of separation, energy dissipation is not limited by the thermodynamic cost of creating new surfaces. In fact, in the regime below the critical crack propagation rate, v^*, the adhesion energy of acrylic PSA-LNs has a small slope, that is, it exhibits a small degree of "bulk" energy dissipation presumed by other researchers and by Equation (2) to be minimal in this limit. The above considerations lead to a

TABLE 6 Comparison of Values of G_0 as a Function of Temperature

Sample designation	G_0 at 0°C (mJ/m^2)	G_0 at 25°C (mJ/m^2)	G_0 at 50°C (mJ/m^2)	$\Delta G_0(T)$ (mJ/m^{2}deg)
PSA-LN-NoAA	76	66	58	0.4
PSA-LN-10DMAEA	194	169	100	1.9
PSA-LN-10AA	177	132	96	1.6
PSA-LN-10AN	241	195	178	1.3

As expected, the values decrease as a function of increasing temperature but the change is greater than expected.

conclusion that "bulk" energy dissipation mechanisms are not activated at v^* but rather become comparable in rate of energy dissipation with intrinsic interfacial adhesion mechanisms at this crack propagation rate.

Another aspect of the observed transition phenomena is the effect of the level of intermolecular interaction at the interface on the magnitude of the critical rate, v^*, and the point in energy space at which the adhesion energy begins to display a higher dependence on v. The data in Table 4 indicate that for those systems in which there is a chance of higher intermolecular interaction (those systems containing polar- and/or hydrogen-bonding monomers), v^* is lower in value than for the system that contains only a modicum of polar interactions, PSA-LN-NoAA. Indeed, G_0 is significantly higher for the PSA-LNs that contain the polar- or hydrogen-bonding monomers. At the rates above v^*, adhesion energy follows a much steeper power law dependence than it does in the regime below v^*. Therefore, even a relatively small change in the extent of the intrinsic regime results in a significantly greater effect in adhesion energy at higher rates. Furthermore, any such variation becomes even more pronounced because changes in v^* are coupled to some extent with changes in the intrinsic adhesion level, G_0. If the transition occurs at a lower critical rate v^*, it is also positioned higher on the adhesion energy scale due to higher intrinsic energy, G_0. In other words, the point of take-off into steep power law behavior changes its position simultaneously in terms of rate and initial adhesion energy, depending on the level of intermolecular interaction at the interface. It was our hope to show the dependence of v^* on intermolecular interactions, but the variance in the data could not support that hypothesis except in the crudest terms.

Ahn and Shull [9] also examined systems that are similar to those in this study. These workers fit their data to Equation (2) to obtain values of G_0 and v^*. We were unable to fit our data to Equation (2)

because of the rather sharp transition between low-rate and high-rate data. (See Figures 6 and 7 for PSA-LN-NoAA and PSA-LN-10AN.) Ahn and Shull did not observe such a sharp transition. In addition, Ahn and Shull's measurements were primarily between acrylic hemispheres and other materials, such as glassy PMMA, and not to themselves. Thus, their work is difficult to compare with ours. However, in general terms, our v^* and G_0 values are on the same order of magnitude as those obtained by Ahn and Shull. The reason why they do not observe a sharp transition in adhesion energy as a function of rate but we do is not discernable from the available information. These workers did not examine temperature dependence.

The critical rate, v^*, also provides an insight into the physical nature of the intermolecular interactions at the interface. The temperature dependence of v^* allows us to calculate activation energies for the physical processes describing the adhesion response (see Figure 9). As shown in Table 5, the activation energies, $Q_A(v^*)$, are relatively low. They are, in fact, on the order of magnitude of van der Waals interactions. The impact of these interactions on self-adhesion is evident from Tables 4 and 5. Among the four acrylic systems tested, the neutral PSA-LN-NoAA system is at the lowest level of thermodynamic work of adhesion and intrinsic adhesion energy and, in fact, W_A and G_0 are very similar for this system. In contrast, PSA-LN-10AN has the highest G_0 and the largest difference between $W_A$and G_0. The remaining PSA-LN-10AA and PSA-LN-10DMAEA fall in between due to the hydrogen-bonding ability of carboxyl group and the lower polarity (in comparison with a cyano group) of the amine functionality. Also, v^* for the systems containing polar monomer is measurably less than that for the system with minimal polar interactions.

The fact that both $Q_A(v^*)$ and $E_A(a_T)$ rank in the same order (see Table 5) reinforces the argument that the addition of polar modifiers affects surface properties as well as bulk properties. Examples of the affected intermolecular mechanisms could be interchain friction due to the side groups or the thermodynamic cost of conformational changes in the network's backbone and dangling ends. Furthermore, in line with expectation that the presence of bulkier, more flexible side groups with greater free volume should reduce the activation energy of viscous flow is confirmed by the ranking of the $E_A(a_T)$ values among the four systems tested. Thus, PSA-LN-10DMAEA does have the lowest activation energy in contrast to PSA-LN-10AN, an elastomer modified with a small, stiff, polar cyano side group.

Ghatak and coworkers [16] examined the temperature dependence of the crack propagation rate in terms of an activated complex formalism:

$$G^{1/2} = \frac{\Sigma_0}{2k_s}\left[\left(\frac{kT}{\lambda}\right)\ln\left(\frac{k_s v\lambda\tau\alpha}{nkT}\right)\right] \quad (5)$$

where G and v are as defined previously, k is Boltzmann's constant, T is the absolute temperature, Σ_0 is the areal bridging density of polymer across the crack opening, k_s is the spring constant for that bridging polymer chain, λ is the activation length of a bond in the polymer chain, τ is the relaxation time of bond dissociation, and α is the slope of the crack face. Ghatak *et al.* [16] show linear plots of $G^{1/2}$ *versus* ln v for systems based upon PDMS. Attempts to fit our data to Equation (5) using estimated values of the necessary parameters did not work; our data is linear in log G *versus* v below v^* and is linear in log G *versus* log v above v^*. To be sure, the assumptions used to derive Equation (5) are not necessarily applicable in our system. That is, the elastic networks used in this work will, for the most part, be unable to provide polymer chains to cross the interface. Although the above-described theory does properly account for the temperature dependence of our adhesion energy data, the remainder of our data is not modeled by Equation (5).

SUMMARY

Contact mechanics of acrylic pressure-sensitive adhesive-like networks were examined at three different temperatures over a range of submicron-per-second rates of interfacial separation. Self-adhesion energies measured as a function of crack propagation rate were found to exhibit a transition to markedly stronger rate dependence above a certain critical rate of crack propagation, v^*. For each of the four systems tested, this rate was found to be a thermally activated parameter. To our knowledge, the above finding is the first of its kind to be reported in the field of polymer adhesion.

A graphical summary of our findings can be found in Figure 10. As temperature increases, the dependence of the adhesion energy on the crack propagation rate shifts to the right (higher rates) and down (lower energy). As the level of intermolecular interaction in the bulk and interface increases, the dependence of adhesion energy on crack propagation rate seems to shift to the left (lower rates) and up (higher energy.) We also found that there is a measurable dependence of G on v at rates below v^*, a finding that is difficult to model using Equation (2).

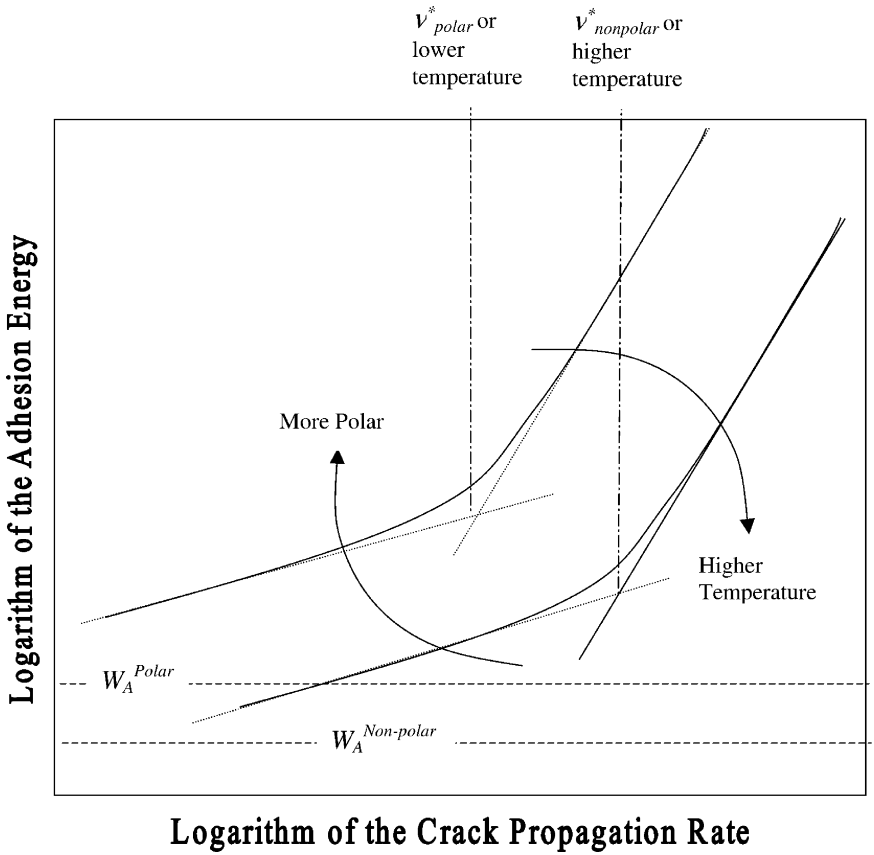

FIGURE 10 Generalized schematic of PSA-LN adhesion, showing a thermally activated transition characterized by change in power law index at a critical or characteristic rate, v^*. In general, as the system becomes more polar, the dependence shifts to the left and up. As the temperature of measurement goes up, the dependence shifts to the right and down.

The activation energy determined from the dependence of the critical crack propagation rate on temperature was found to be on the order of the energy to break van der Waals attractions (~2 kcal/mole.) mole.) The materials used in this study are chemically very similar to the chemistry of commercial acrylic pressure-sensitive adhesives, albeit at a much higher crosslink density than that used in commercial PSAs. Thus, despite the fact that the magnitude of van der Waals attractions are quite low, they are the source of the quite measurable adhesive bond strength of pressure-sensitive adhesives.

REFERENCES

[1] Gent, A. N. and Schultz, J., *J. Adhesion* **3**, 281 (1972).
[2] (a) Andrews, E. H. and Kinloch, A. J., *Proc. Roy. Soc. London* A. **332**, 385 (1973).
(b) Andrews, E. H. and Kinloch, A. J., *Proc. Roy. Soc. London* A **332**, 401 (1973).
(c) Gent, A. N. and Kinloch, A. J., *J. Polym. Sci., Part A-2* **9**, 659 (1971).
[3] Hertz, H., *J. Reine. Angew. Math*. **92**, 156 (1882).
[4] Bradley, R. S., *Philos. Mag*. **13**, 853 (1932).
[5] Johnson, K. L., Kendall, K., and Roberts, A. D., *Proc. Roy. Soc., Ser. A* **324**, 301–313 (1971).
[6] Derjaguin, B. V., Muller, V. M., and Toporov, Y. P., *J. Coll. Interface Sci*. **53**, 314 (1975).
[7] Maugis, D., *J. Colloid Interface Sci*. **150**, 243–269 (1992).
[8] Lin, Y.-Y. and Hui, C. Y., *J. Polym. Sci., Part B: Polymer Physics* **40**, 772–793 (2002).
[9] (a) Ahn, D. and Shull, K. R., *Macromolecules* **29**, 4381 (1996).
(b) Ahn, D. and Shull, K. R., *Langmuir* **14**, 3637 (1998).
(c) Ahn, D. and Shull, K. R., *Langmuir* **14**, 3646 (1998).
(d) Shull, K. R., *Mat. Sci. Eng*. **R36**, 1 (2002).
[10] (a) Li, L. H., Tirrell, M., Korba, G. A., and Pocius, A. V., *J. Adhesion* **76**, 307–334 (2001).
(b) Li, L. H., Macosko, C., Korba, G. L., Pocius, A. V., and Tirrell, M., *J. Adhesion* **77**, 95–123 (2001).
[11] Ulrich, E. W., U. S. Patent 2,884,126 (1959).
[12] Rudin, A., *The Elements of Polymer Science and Engineering* (Academic Press, San Diego, CA, 1999), p. 149.
[13] Falsafi, A., Tirrell, M., and Pocius, A. V., *Langmuir* **16**, 1816–1824 (2000).
[14] Maeda, N., Chen, N. H., Tirrell, M., and Israelachvili, J. N., *Science* **297**, 379–382 (2002).
[15] Chaudhury, M. K. and Owen, M. J., *J. Phys. Chem*. **97**, 5722 (1993).
[16] Ghatak, A., Vorvolakos, K., She, H., Malotky, D. L., and Chaudhury, M. K., *J. Phys. Chem. B* **104**, 4018 (2000).
[17] Wu, S., *Polymer Interface and Adhesion* (Marcel Dekker, New York, 1982), Chap. 3.